





# Longitudinal Investigation of Brain and Spinal Cord Pericytes After Inducible PDGFRβ<sup>+</sup> Cell Ablation in Adult Mice

<sup>1</sup>Koç University Research Center for Translational Medicine (KUTTAM), Koç University, İstanbul, Türkiye | <sup>2</sup>Department of Neurology, Koç University, İstanbul, Türkiye | <sup>3</sup>Department of Physiology, Bakırçay University, İzmir, Türkiye | <sup>4</sup>School of Medicine, Koç University, İstanbul, Türkiye | <sup>5</sup>Department of Molecular Medicine, Aziz Sancar Institute of Experimental Medicine, İstanbul University, Istanbul, Türkiye | <sup>6</sup>Department of Neuroscience, Aziz Sancar Institute of Experimental Medicine, İstanbul University, Istanbul, Türkiye

Correspondence: Atay Vural (atayvural@ku.edu.tr)

Received: 29 January 2025 | Accepted: 3 February 2025

**Funding:** This study was funded by TÜBİTAK (project no: 116S252). Dr. Atay Vural was supported by TÜBİTAK 2236 Co-Funded Brain Circulation Scheme 2 (Project No: 119C018).

 $\textbf{Keywords:} \ brain \ | \ cortex \ | \ inducible \ PDGFR\beta^+ \ cell \ ablation \ | \ regeneration \ | \ spinal \ cord \ | \ tamoxifen \ | \ transgenics \ decreases \ decrea$ 

## **ABSTRACT**

Central nervous system (CNS) pericytes play crucial roles in vascular development and blood–brain barrier maturation during prenatal development, as well as in regulating cerebral blood flow in adults. They have also been implicated in the pathogenesis of numerous neurological disorders. However, the behavior of pericytes in the adult brain after injury remains poorly understood, partly due to limitations in existing pericyte ablation models. To investigate pericyte responses following acute ablation and characterize a novel rodent model for pericyte research, we developed a tamoxifen-inducible PDGFR $\beta$ + cell ablation model by crossing *PDGFR\beta-P2A-CreER*<sup>T2</sup> and *Rosa26-DTA176* transgenic mouse lines. Using this model, we studied the effects of different tamoxifen doses and conducted histological examinations 15 and 60 days post-injection to assess the impacts of PDGFR $\beta$ + cell ablation in both acute and chronic phases, respectively. Our results demonstrate that a low dose of tamoxifen effectively ablates PDGFR $\beta$ + cells of the CNS in mice without reducing survival or causing significant systemic side effects, such as weight loss. Additionally, we found that the extent of PDGFR $\beta$ + cell depletion varies between the cortex and the spinal cord, as well as between the gray and white matter regions of the spinal cord. Importantly, we observed that both pericyte coverage and numbers increased in the weeks following acute ablation, indicating the regenerative capacity of CNS pericytes in vivo. This study offers a valuable tool for future studies on the role of pericytes in neurological disorders by overcoming the limitations of constitutive pericyte ablation models and providing its longitudinal characterization in the CNS.

Abbreviations: ANOVA, analysis of variance; AVL, average vessel length; BBB, blood-brain barrier; BSA, bovine serum albumin; Cat. No., Catalog number; CNS, central nervous system; CreER, Cre recombinase fused with estrogen receptor; Cspg4, chondroitin sulfate proteoglycan 4; CT, cycle threshold; DAPI, 4',6-diamidino-2-phenylindole; DF, degree of freedom; DFn, degree of freedom for numerator; DFA, day post-injection; DPBS, dulbecco's phosphate-buffered saline; DT, diphtheria toxin; DTA, diphtheria toxin A variant; DTA176, attenuated diphtheria toxin A variant; EDTA, ethylenediaminetetraacetic acid; GAPDH, glyceraldehyde 3-phosphate dehydrogenase; H&E, hematoxylin and eosin; HRP, horseradish peroxidase; iDTR, inducible diphtheria toxin receptor; JD, junction density; MIP, maximum intensity projection; NG2, neuroglial antigen 2; NGS, normal goat serum; OCT, optimal cutting temperature compound; P2A, 2A peptide from porcine teschovirus-1; PBS, phosphate-buffered saline; PDGF-B, platelet-derived growth factor-B; PDGFRB, platelet-derived growth factor beta; PFA, paraformaldehyde; RRID, research resource identifier; RT-qPCR, real-time quantitative polymerase chain reaction; SD, standard deviation; SEM, standard error of the mean; TAM, tamoxifen; TBS, tris-buffered saline; VPA, vessel percentage area; vSMCs, vascular smooth muscle cells.

Atay Vural and Yasemin Gürsoy-Özdemir contributed equally to this work.

This is an open access article under the terms of the Creative Commons Attribution-NonCommercial License, which permits use, distribution and reproduction in any medium, provided the original work is properly cited and is not used for commercial purposes.

© 2025 The Author(s). Journal of Neurochemistry published by John Wiley & Sons Ltd on behalf of International Society for Neurochemistry

## 1 | Introduction

Pericytes are mural cells located on the abluminal side of the microvessels and are recruited to the vessel surface by plateletderived growth factor-B (PDGF-B) secreted from endothelial cells. These cells detect PDGF-B through the platelet-derived growth factor receptor \( \beta \) (PDGFR\( \beta \)), which is widely recognized as a critical and indispensable marker in pericyte research (Winkler et al. 2010; Berthiaume et al. 2018). While PDGFRβ is also expressed in other cell types, such as vascular smooth muscle cells (vSMCs) and perivascular fibroblasts, pericytes exhibit markedly higher levels of Pdgfr\beta expression compared to these cell types (Vanlandewijck et al. 2018), solidifying its role as a reliable target for genetic manipulation in functional studies. To strengthen the specificity and accuracy of pericyte identification, researchers frequently combine Pdgfb/Pdgfrβ-based methodologies with complementary markers, including CD13 (aminopeptidase N) (Crouch et al. 2015) and NG2 (neuroglial antigen 2) (Ozerdem et al. 2002).

PDGFRβ-positive pericytes are distributed throughout the body in tissues such as the brain, heart, cochlea, and adipose tissue, where they contribute to vascular stability, tissue repair, and metabolic regulation (Sandow et al. 2023). Notably, the pericyte/endothelial cell ratio is highest in the retina and brain (Armulik et al. 2011; Trost et al. 2016; Sweeney et al. 2016). In the healthy central nervous system (CNS), pericytes are pivotal for the maturation of the blood-brain barrier (BBB; Daneman et al. 2010; Armulik et al. 2010), regulation of blood flow (Peppiatt et al. 2006; Hartmann et al. 2021), and angiogenesis (Nehls et al. 1992; Stapor et al. 2014). Disruptions in these functions of pericytes have been strongly implicated in the pathogenesis of several neurological disorders, such as stroke (Yemisci et al. 2009; Hall et al. 2014), multiple sclerosis (Kaushik et al. 2021; Torok et al. 2021; Sekerdag-Kilic et al. 2023), Alzheimer's disease (Sagare et al. 2013) and CNS trauma (Goritz et al. 2011; Holl et al. 2024). Previous research, including our own, has demonstrated that pericyte dysfunction or deficiency under pathological conditions leads to microcirculation deficits (Yemisci et al. 2009; Kisler et al. 2017, 2020) and BBB leakage (Winkler, Sengillo, Bell, et al. 2012; Bell et al. 2010), and can contribute to scar formation (Holl et al. 2024) and neuroinflammation (Rustenhoven et al. 2017).

To elucidate the roles of pericytes in CNS physiology and pathology, researchers have employed various genetic approaches to ablate these cells. However, conventional pericyte ablation models are often limited by their reliance on constitutional genetic modifications, which disrupt critical signaling pathways during embryonic development and introduce confounding developmental abnormalities. For instance, one of the earliest models involves a complete disruption of the Pdgfb gene, which resulted in embryonic lethality due to severe vascular abnormalities (Leveen et al. 1994). Later, heterozygous mice  $(Pdgfb^{+/-})$  were shown to exhibit partial pericyte loss and capillary irregularities such as microaneurysm, cylindrical dilations, and enhanced endothelial cellularity (Lindahl et al. 1997). When Pdgfb was deleted specifically in endothelial cells, mice survived into adulthood but exhibited inconsistent pericyte coverage reduction and persistent vascular abnormalities (Enge et al. 2002). Another approach for generating mice with partial pericyte depletion was to disrupt the retention motif of PDGF-B (Lindblom 2003), which resulted in BBB breakdown and increased leukocyte adhesion molecule expression (Armulik et al. 2010; Torok et al. 2021). An alternative approach involving the complete knockout of  $Pdgfr\beta$  gene  $(Pdgfr\beta^{-/-})$  also resulted in embryonic lethality, while heterozygous mice  $(Pdgfr\beta^{+/-})$  showed partial pericyte deficiency and associated vascular and neurodegenerative changes (Bell et al. 2010; Tallquist et al. 2003; Watson et al. 2020). As another strategy, point mutations were introduced into the PDGFR\$, resulting in partial pericyte loss and leading to increased BBB permeability and disrupted blood flow (Tallquist et al. 2003; Montagne et al. 2018). While these anomalies were attributed to pericyte loss, they did not clearly establish whether the observed outcomes stemmed from developmental disruptions caused by early genetic manipulations, secondary complications from lifelong pericyte absence, or the specific functional roles of pericytes in the adult brain.

These limitations have driven the development of inducible pericyte ablation models, which enable cell-type-specific and temporally controlled manipulation of Pdgfb/Pdgfrβexpressing cells. Nikolakopoulou et al. (2019) developed a pericyte-specific, inducible ablation model using a doublepromoter approach targeting  $Pdgfr\beta$  and Cspg4. In this model, mice were crossed with iDTR mice (Buch et al. 2005) and tamoxifen was administered to the offspring, leading to the expression of the diphtheria toxin (DT) receptor in cells carrying the  $Pdgfr\beta$  and Cspg4 promoters. Subsequent injection of DT resulted in a reduction of pericytes. This model effectively demonstrated BBB breakdown and neurovascular uncoupling in adult mice following pericyte ablation, which was associated with neurodegeneration. Although this model is valuable for studying CNS pericytes, it is limited in scope and cannot be easily adapted for examining pericyte dynamics in other organs. Additionally, it requires the use of specific double-promoter mice, which are not commercially available, and relies on extrinsic DT injections that may induce systemic adverse effects (Buch et al. 2005). This reliance on DT complicates experimental designs and restricts compatibility with co-administration of other compounds, such as those used in experimental autoimmune encephalomyelitis models.

Another inducible approach, used by Vazquez-Liebanas et al. involved developing an endothelial-specific, tamoxifen-inducible deletion of Pdgfb by crossing  $Pdgfb^{flox/flox}$  or  $Pdgfb^{flox/-}$  mice with Cdh5(PAC)-CreERT2 mice. In the 2-month-old adult progeny, they imposed tamoxifen-inducible Pdgfb deletion, which eventually caused a slowly progressive pericyte loss when they reached the age of 12-18 months. Using this model, the authors confirmed the role of pericytes in the maintenance of BBB and the prevention of its selective permeability. They additionally showed that adult-induced loss of PDGF-B does not lead to vessel dilation, impaired arteriovenous zonation, or the formation of microvascular calcifications, unlike those observed in the constitutive developmental PDGF-B loss of function animal models (Vazquez-Liebanas et al. 2022). However, due to its indirect approach through endothelial signaling, this model is slowly showing its effect on pericytes and is not suitable for studying the effects of acute pericyte ablation, particularly in younger mice.

Here, we aimed to develop and characterize a novel tamoxifeninducible acute PDGFR $\beta$ <sup>+</sup> cell ablation model that overcomes these challenges. We leveraged the intrinsic attenuated DTA176 expression system with PDGFRβ-P2A-CreERT2 (JAX Mice, RRID: IMSR\_JAX:030201). This approach enables precise and efficient ablation of PDGFRβ+ cells while providing temporal control and eliminating the need for extrinsic DT administration. We tested various tamoxifen doses to determine the optimal dose that induces effective PDGFRβ+ cell ablation without causing significant systemic adverse effects. Furthermore, we performed detailed longitudinal analyses of pericyte depletion and recovery across distinct CNS regions while maintaining the integrity of normal developmental processes. We showed that PDGFRβ+ cells of the CNS are partially replenished in vivo after the acute PDGFR\$\beta^+\$ cell ablation period is over. This model represents a significant step forward in the study of pericytes, enabling precise investigations into their roles in homeostasis and disease. Its adaptability for various CNS and systemic applications positions it as a valuable tool for future research.

#### 2 | Materials and Methods

#### 2.1 | Animals

All procedures of this study were approved by the Koç University Ethics Committee (no: 2019. HADYEK.021). The mice were kept in a regulated facility at  $22^{\circ}\text{C} \pm 2^{\circ}\text{C}$  with a 12-h light/dark cycle to ensure optimal acclimatization before the experiments began. The animals were housed in groups of no more than five per cage and had continuous access to food and water.

PDGFRβ-P2A-CreER<sup>T2</sup> (JAX Mice, RRID: IMSR\_JAX:030201) and Rosa26-DTA176 (JAX Mice, RRID: IMSR JAX:010527) transgenic mice were used for this study. The PDGFRβ-P2A- $CreER^{T2}$  line was developed by Cuervo et al. (2017). The P2A gene allows "ribosome skipping" between the  $Pdgfr\beta$  and  $CreER^{T2}$ coding sequences, resulting in the production of related proteins at similar expression levels. The Rosa26-DTA176 line was developed by Wu et al. (2006). We chose this line because DTA176 is an attenuated form of fragment A of the diphtheria toxin (DTA). Once inside a cell, one molecule of DTA is sufficient to kill the target cell, whereas DTA176 is toxic at approximately 100-200 molecules per cell. This approach mitigates potential issues related to the leaky expression of DT before Cre-mediated activation (Wu et al. 2006). To segregate mice into appropriate experimental cohorts, after mating of the PDGFRβ-P2A-CreER<sup>T2</sup> and Rosa26-DTA176 lines, the offsprings were genotyped to identify the inducible CreER+ and noninducible CreER- transgenic mice. The primer sequences and the details of the touchdown PCR are given in Tables S1 and S2, respectively.

## 2.2 | Inclusion and Exclusion Criteria

No predetermined exclusion criteria were applied at the beginning of the study. However, animals exhibiting severe health deterioration (e.g., > 20% weight loss, signs of distress, or immobility) were humanely euthanized according to institutional ethical guidelines.

Based on observations from the acute phase (Day 15) of the CreER<sup>+</sup> 5X tamoxifen group, significant health concerns were noted. As a precautionary measure, 12 mice (six males, six females) from the chronic phase CreER<sup>+</sup> 5X tamoxifen group were euthanized before their scheduled termination to prevent unnecessary suffering.

Additionally, two mice (one male, two females) from the acute phase CreER+ 5X tamoxifen group were found dead in their cages before the planned termination day. These animals were excluded from the study and were not replaced.

The final analysis was conducted on 79 animals, ensuring a balanced distribution across experimental conditions.

# 2.3 | Tamoxifen Administration for Induction of PDGFR $\beta^+$ Cell Ablation

Tamoxifen (Sigma-Aldrich, CAS No. 10540-29-1) was prepared as a 10 mg/mL solution in corn oil and administered intraperitoneally to mice at 100 mg/kg/day for 2 (2X group), 3 (3X group), or 4 (5X group) days depending on their experimental group. Tamoxifen treatment initiated the CreER-mediated genetic recombination process only in the CreER+ mice, selectively ablating  $Pdgfr\beta$ -expressing cells through the induced expression of the DTA176. On the other hand, CreER- mice were also treated with the same doses of tamoxifen and used as a control group.

# 2.4 | Experimental Design

The experimental setup included a total of 93 mice (48 males and 45 females) aged between 8 and 16 weeks. Each mouse was marked with an identification number using ear notching. No formal statistical sample size calculation was performed a priori. Instead, we based our experimental design on previously published studies using similar pericyte ablation models and neurovascular investigations (Berthiaume et al. 2018; Kisler et al. 2017; Montagne et al. 2018; Nikolakopoulou et al. 2019; Winkler, Sengillo, Sullivan, et al. 2012). Mice were assigned to experimental groups using a block randomization method to ensure balanced distribution across groups, and randomization was stratified by sex and body weight to prevent potential confounding effects. Mice were systematically divided into CreER+ and CreER- groups depending on their genotyping results (56 CreER+ [30 females, 26 males] and 37 CreER- [18 females, 19 males]). Within these divisions, mice were further randomly and equally allocated into subgroups based on the duration of tamoxifen treatment (2X, 3X, or 5X tamoxifen treatment; 34, 33, and 14 mice, respectively). The 2X tamoxifen group included 17 females and 17 males, the 3X group had 17 females and 16 males, and the 5X group had 6 females and 8 males.

Follow-ups on these mice were conducted over 15 days (acute phase, 54 mice: 27 females, 27 males) or 60 days (chronic phase, 39 mice: 18 females, 21 males), with body weight tracking. After the completion of the experiments, animals were euthanized following institutional animal ethics guidelines. First, animals from each group were anesthetized with

a cocktail of 100 mg/kg ketamine (Sigma-Aldrich, CAS No. 1867-66-9) and 20 mg/kg xylazine (Sigma-Aldrich, CAS No. 7361-61-7) injection. Transcardial perfusion was carried out using ice-cold phosphate-buffered saline (PBS, Sigma-Aldrich, Cat. No. D8537), followed by fixation with 4% paraformaldehyde (PFA) (Sigma-Aldrich, Cat. No. 158127, CAS No. 30525-89-4) in PBS, and tissues were extracted for histological and molecular analyses of the brain and spinal cord (56 mice: 29 females, 27 males). For the tissues preserved for further quantitative PCR analysis, a randomly selected group of mice from each group (23 mice: 12 females, 11 males) was euthanized by decapitation, and the CNS tissues were snap-frozen by exposure to liquid nitrogen. Additionally, 14 mice (7 females, 7 males) were excluded from further analyses due to experimental constraints.

#### 2.4.1 | Blinding Procedures

Blinding was implemented during data collection and analysis to minimize bias. While experimenters responsible for administering tamoxifen and conducting animal procedures were aware of group allocations due to necessary treatment differences, blinding was applied in all subsequent analyses. For histological and immunofluorescence experiments, tissue samples were coded and anonymized before sectioning and staining, ensuring that imaging and quantification were conducted without knowledge of the experimental conditions. In qRT-PCR analysis, data collection was carried out by an investigator who was unaware of sample identities. Behavioral assessments were conducted with mice labeled by coded numbers, so the experimenter remained blinded to treatment conditions while recording data.

When blinding was not feasible, such as during tamoxifen administration and euthanasia, potential bias was minimized by following standardized protocols and relying on objective quantitative assessments.

## 2.5 | Immunohistochemistry

After fixation of tissues in 4% PFA at 4°C for 12h, brain and cervical, thoracic, lumbar, and sacral segments of the spinal cord tissues were cryoprotected using 10%, 20%, and 30% sucrose solutions until they reached equilibrium. For cryosectioning, tissues were embedded in the optimal cutting temperature compound (OCT) and rapidly frozen using liquid nitrogen vapor. Cryosections of the brain were prepared at 30 µm thickness in a free-floating manner, whereas spinal cord tissues were sectioned at  $20\,\mu m$  on slides. Four serial sections, spaced  $100\,\mu m$ apart, were collected per sample. For immunofluorescence, sections underwent blocking and permeabilization with a solution containing 5% normal goat serum (NGS) (Sigma-Aldrich, Cat. no. G9023), 2% bovine serum albumin (BSA) (Cat. No. A4919, CAS No. 9048-46-8), and 0.1% Triton X-100 (Sigma-Aldrich, Cat. No. 648466, CAS No. CAS\_9002-93-1) in Dulbecco's phosphatebuffered saline (DPBS) (Sigma-Aldrich, Cat. No. D8537) for 1 h at room temperature. This was followed by overnight incubation at 4°C with primary antibody against CD13 (Bio-Rad, Cat. No. MCA2183) at a 1:100 dilution in the blocking solution. After primary antibody incubation, sections were rinsed in DPBS and then incubated with Alexa Fluor 647-labeled anti-rabbit IgG (Abcam, Cat. No. ab150159) and DyLight 488–conjugated tomato lectin (Vector Laboratories, Cat. No. DL-1174), at 1:200 dilution for 2h at room temperature to visualize pericytes and vasculature, respectively. The stained sections were then mounted using a PBS–glycerol mixture containing Hoechst stain and coverslipped for imaging. All staining procedures were performed in batches that included both the experimental and control groups to minimize technical variability during analysis. Imaging was performed on a Leica DMI8 SP8 Confocal Microscope, capturing 6–8 random cortical areas from nonadjacent brain sections approximately  $100\,\mu m$  apart at  $20\times$  magnification and 8–12 areas across white and gray matter at  $40\times$  magnification from different spinal cord segments.

## 2.6 | Image Analysis

For pericyte coverage analysis,  $10\text{-}\mu\text{m}$  thick z-stack images were obtained with a  $2\text{-}\mu\text{m}$  step size with a confocal microscope. Then, maximum intensity projection (MIP) images were obtained and transformed into 8-bit pictures for each channel. Following the Gaussian filter ( $\sigma$ =2), pictures were masked with triangle thresholding. Particles smaller than 50 pixels² in size were eliminated to exclude nonspecific staining. Finally, the pericyte coverage was calculated by dividing the integrated density of the CD13 signal by the integrated density of the tomatolectin signal. A custom MATLAB code was written to automate these processes and to avoid biased manual adjustments.

Pericytes were manually counted using ImageJ on the same MIP images. CD13-positive signals that overlapped with a Hoechst-stained nucleus (blue) and were located on a tomatolectin–stained vessel (green) were identified as pericytes. Both pericyte coverage and numbers were normalized to the average of the control groups for each tamoxifen dose.

For vessel parameter analysis, images from the tomato-lectinstained channel were exported to ImageJ. MIP images were then generated and converted to 8-bit grayscale. A Gaussian blur ( $\sigma$ =2) was applied, followed by triangle thresholding to delineate vascular structures. A binary mask was created, excluding background elements smaller than 20 square pixels to isolate the stained vessels. The resultant binary images, as illustrated in Figure S1, were imported into AngioTool software for quantitative vascular analysis. The parameters assessed included vessel percentage area (VPA), junction density (JD), and average vessel length (AVL), providing comprehensive metrics of the vascular network.

# 2.7 | Real-Time Quantitative Polymerase Chain Reaction (RT-qPCR)

Snap-frozen brain tissues were processed for RNA isolation using the RNA Miniprep Plus Kit (Zymo Research, Cat. No. R1055) following the manufacturer's protocol. From the isolated RNA, 500 ng was used as a template for cDNA synthesis through reverse transcription with random primers. RT-qPCR analyses were subsequently performed using the miScript SYBR Green PCR Kit (Qiagen, Cat. No. 218073) on the LightCycler

480 System (Roche Diagnostics). GAPDH cDNA served as an internal control to normalize expression levels. The relative expression levels of the target genes were determined by calculating the difference in cycle threshold ( $\Delta$ CT) values between GAPDH and the target mRNA, followed by quantification using the 2 $^{\text{-}}$ (- $\Delta$ CT) method. Each assay was conducted in triplicate and repeated across three independent experiments to ensure reliability and reproducibility. The following *forward* (*FW*) and *reverse* (*RV*) *primers* were used:

PDGFRβ (mouse)

Forward: TTGCTGATGAAGGTCTCCCA
Reverse: TTGCTGTGGCTCTTCTTGGA

CD31 (mouse)

Forward: ACACACTTGGTCCAGGAGTT
Reverse: TCACTGCTTTGCTTGGAGGT

#### 2.8 | Behavioral Tests

Y-maze spontaneous alternation test was used to assess the spatial recognition memory of the mice. The Y-maze apparatus consisted of arms, each measuring 35cm in length, 20cm in depth, and 6cm in width, with a white finish. Each mouse's behavior was observed and recorded for 5 min following its release into the maze. To maintain environmental consistency and eliminate olfactory cues, the maze was thoroughly cleaned with a 10% ethanol solution and air-dried between sessions. Video recordings from the experiment were manually analyzed to track the frequency and pattern of arm entries. A "spontaneous alternation" was defined as the sequence in which a mouse entered all three arms consecutively without reentering a previously visited arm. The Y-maze performance score, reflecting the animal's spatial working memory, was calculated by dividing the number of spontaneous alternations by the total number of arm entry triads. Mice with fewer than 5 total arm entries were excluded from the analysis due to insufficient mobility.

The locomotor activity of the mice was evaluated using Kondziela's inverted screen (grip strength) test. Each mouse was initially placed at the center of a  $30 \times 30\,\mathrm{cm}$  screen made of 1 mm squared mesh. To begin the test, the screen was gently inverted, encouraging the mouse to grip the mesh to prevent falling. This procedure was repeated three times per mouse, and the duration of the grip was recorded either until the mouse fell or until a maximum time of 90 s was reached. The endurance time, defined as the length of time each mouse held onto the inverted screen before falling, was recorded for each trial. The average holding time was then calculated and compared between the experimental and control groups to assess differences in locomotor capabilities.

# 2.9 | Statistical Analysis

All statistical analysis was performed by GraphPad Prism 10 (Version 10.2.0). Survival analysis was conducted using the

log-rank (Mantel–Cox) test. The difference in body weight between groups was analyzed using two-way ANOVA followed by Bonferroni tests. Student's *t*-test was used to compare pericyte coverage, count, vascular parameters, and motor and memory functions between groups. P values less than 0.05 were considered statistically significant.

No formal outlier detection test was conducted in this study, and no data points were excluded as outliers. All collected data were included in the final analysis. Prior to applying parametric tests, data distribution was assessed for normality using the Shapiro–Wilk test. Statistical details for each figure are given in the Supplementary pdf (Supplementary Table S3–S10).

#### 3 | Results

# 3.1 | Acute Ablation of PDGFR $\beta^+$ Cells Results in Dose-Dependent Changes in Body Weight and Survival

To create an inducible PDGFRβ+ cell ablation model, we crossbred two transgenic mouse lines: PDGFRβ-P2A-CreER<sup>+/-</sup> and Rosa26- $DTA176^{+/+}$ . The  $PDGFR\beta$ -P2A- $CreER^{T2}$  line expresses the  $CreER^{T2}$  complex under the  $Pdgfr\beta$  promoter, which activates only upon tamoxifen administration. This activation facilitates the excision of loxP-flanked sequences in Pdgfr\beta expressing cells. As a mating partner to this line, the Rosa26-DTA176 line contains a loxP-flanked stop codon sequence upstream of the attenuated diphtheria toxin A (DTA176) transgene, controlled by the constitutive Rosa26 promoter. Tamoxifen-induced Cre recombinase excises the stop codon sequence, allowing DTA expression specifically in PDGFR $\beta$ <sup>+</sup> cells. This strategy allowed us to selectively ablate PDGFR $\beta$ <sup>+</sup> cells in the progeny, with  $CreER^+$  progeny serving as the PDGFR $\beta^+$  cell ablation group upon tamoxifen administration, while CreER- mice served as controls in characterization experiments (Figure 1a).

We first investigated the effect of varying tamoxifen doses to identify the optimal dosage by administering  $100\,\mathrm{mg/kg/day}$  tamoxifen for 2, 3, or 5 consecutive days (2X, 3X, and 5X groups, respectively) by assessing both acute (Day 15) and chronic (Day 60) outcomes (Figure 1b). Notably, survival analysis demonstrated a significant impact of the highest tamoxifen dose (5X) on the survival of mice (p < 0.0001; Figure 1c). Mice in the 5X group started to have a sick phenotype 12 days post-injection, and none of them survived beyond 3 weeks (Figure S2), whereas all animals in the 2X and 3X groups remained viable throughout the 60-day observation period. Autopsies could be performed on a few mice immediately after their death and revealed large, swollen, dark-colored intestines (Figure S3). As all animals in the 5X group died by Day 25, we could make examinations only in the acute phase for this group.

There were significant body weight differences between PDGFR $\beta^+$  cell-ablated and CreER<sup>-</sup> control mice in the 3X and 5X tamoxifen groups in the acute phase, but not in the 2X tamoxifen group (Figure 1d). In the 3X tamoxifen group, weight loss was evident on Day 4 and became markedly significant by Day 7 (p<0.0001), culminating in a 17% difference by Day 15 (Figure 1d). Similarly, the 5X tamoxifen group showed

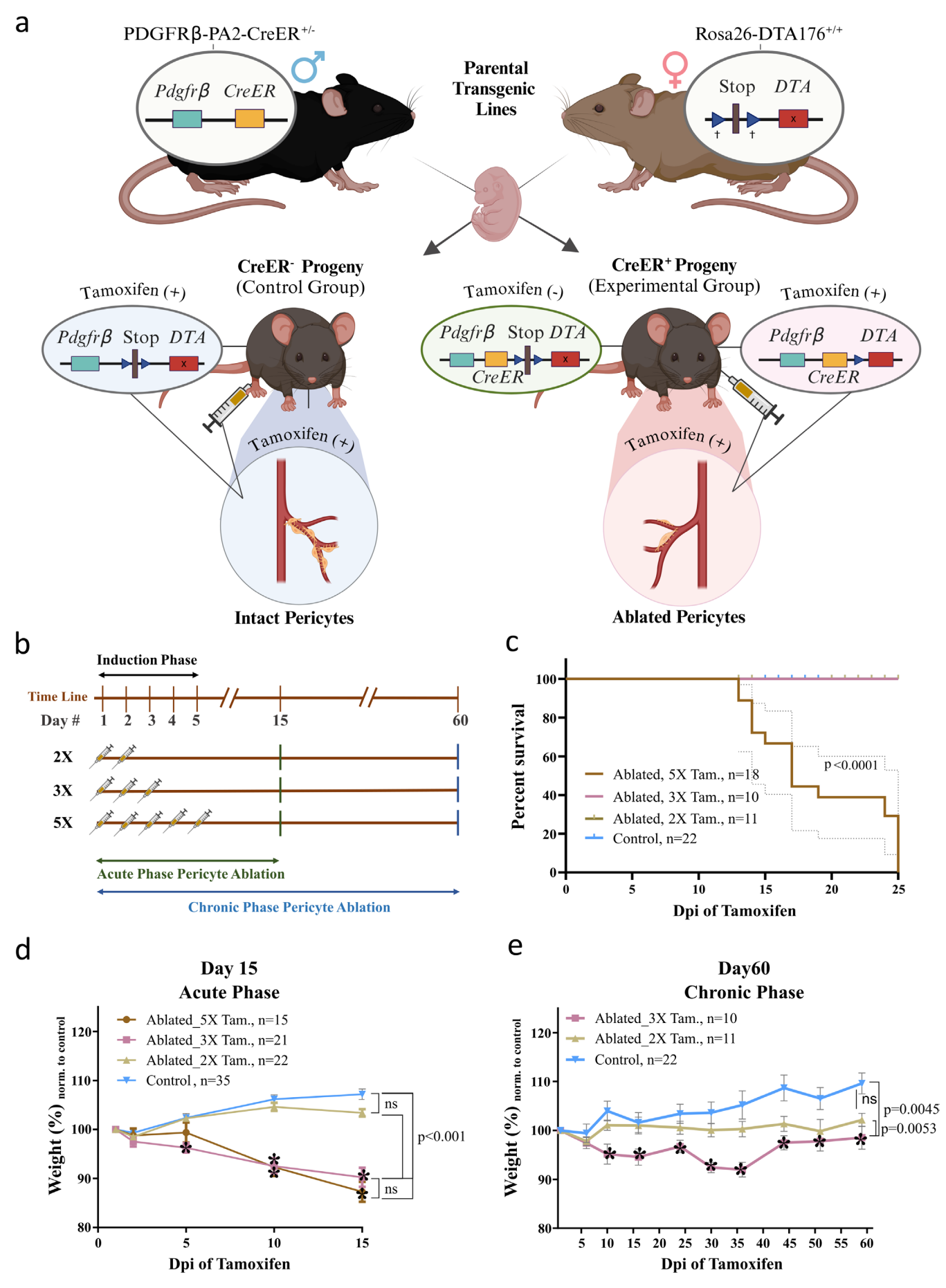


FIGURE 1 | Legend on next page.

FIGURE 1 | Generation of a temporally controlled PDGFRβ<sup>+</sup> cell ablation model in mice and the impact of PDGFRβ<sup>+</sup> cell ablation on body weight. (a) Diagram illustrating the generation of a tamoxifen-inducible and cell type-specific PDGFRβ+ cell ablation model through the crossbreeding of PDGFRβ-P2A-CreER<sup>+/-</sup> and Rosa26-DTA176<sup>+/+</sup> transgenic mouse lines. CreER<sup>+</sup> progeny was used as the PDGFRβ<sup>+</sup> cell ablation group, and CreER<sup>-</sup> progeny served as a control group. Both groups received tamoxifen injections depending on their repetitive dosage group. Created by Biorender. com. (b) Schematic of the tamoxifen induction protocol depicting dosage schedules (2X, 3X, and 5X) and subsequent evaluation time points (Day 15 for acute phase and Day 60 for chronic phase). (c) Kaplan-Meier survival analysis of mice subjected to varying tamoxifen dosages, highlighting the survival impact of post-PDGFRβ+ cell ablation over 25 days. Censorship is indicated by tick marks; p values calculated using Log-rank (Mantel-Cox) test, noted as < 0.0001. Error bars denote 95% confidence intervals. (d-e) Graphs depicting body weight trajectories of control versus pericyte-ablated mice during the acute (15 days) (d) and chronic (60 days) (e) phases post-tamoxifen induction. Data are presented as mean  $\pm$  SEM for n = 10-24 mice per group. Statistical analysis was conducted using two-way repeated measures ANOVA followed by the Benferroni test, with p < 0.05 considered as significant. No significant differences in body weight were detected between the CreER- control groups treated with 2X, 3X, and 5X tamoxifen; thus, these groups were combined for statistical comparison. In the acute phase (d), significant weight differences were observed in the 3X and 5X CreER+ groups compared to controls. In the chronic phase (e), there was a statistically significant difference only between 3X CreER+ mice compared to controls. The 2X group does not show a significant difference in both acute and chronic phases of pericyte ablation. Asterisks denote the statistically significant results of posthoc multiple comparisons conducted to assess weight differences at individual time points compared to the CreER controls. Statistical details are given in Table S3. X = repetitive doses of tamoxifen injection, Tam. = tamoxifen, Dpi = day post-injection, blue  $box = Pdgfr\beta$ , brown box = translational stop sequence, blue arrows (†) = lox P sites, red box with "x" = untranslated DTA, red box = translated DTA, yellow box = Cre recombinase fused with estrogen receptor.

statistically significant weight loss starting from Day 7, reaching a 20% reduction by Day 15 (p < 0.0001).

Long-term monitoring over 60 days revealed that the 3X tamoxifen group maintained lower body weight compared to controls, although a partial weight recovery was observed around 40 days post-tamoxifen injection (Figure 1e). In contrast, the 2X tamoxifen group showed no significant weight differences throughout the observation period. The data suggest a dose-dependent effect of tamoxifen on survival and body weight in  $CreER^+, PDGFR\beta^+$  cell–ablated mice.

# 3.2 | Tamoxifen-Induced Ablation Reveals Regional Variability and Complex Recovery Dynamics of PDGFRβ<sup>+</sup> Cells Throughout the CNS

Immunofluorescence analysis was conducted to assess the degree of PDGFR $\beta^+$  cell ablation in both cortical and spinal regions of mice after various repetitive doses of tamoxifen induction at acute and chronic phases (Figure 2). Quantitative analysis showed an effective reduction in both pericyte coverage and counts in both cortical and spinal cord tissues for each repetitive dosage (Figures 2 and 3).

In the acute phase, pericyte coverage in the cortex decreased by 83%, 81%, and 75% in the 2X, 3X, and 5X tamoxifen-treated mice, respectively, compared to CreER<sup>-</sup> controls (Figure 2a,c). In the chronic phase, cortical pericyte coverage was reduced by 67% and 71% for the 2X and 3X doses, respectively (Figure 2b,c). The analysis of pericyte count in the cortex showed a 58% (in 2X group), 44% (in 3X group), and 55% (in 5X group) decrease compared to controls during the acute phase, and a 31% (in 2X group) and 48% (in 3X group) decrease compared to controls during the chronic phase (Figure 2d). The effectiveness of the ablation was also confirmed at the mRNA level with the target gene *PdgfrB* (Figure S4).

When comparing the effects of different tamoxifen doses on pericyte coverage, no significant differences were observed across the dosages during either the acute or chronic phase (Figure 2e). Notably, despite the decreased survival following the 5X dose, pericyte numbers in the cortex were comparable to those seen with the 2X dose. Interestingly, the 3X dose caused a less pronounced reduction in pericyte count in the acute phase compared to both the 5X and 2X doses. However, in the chronic phase, the pericyte count was significantly lower in the 3X group compared to that in the 2X dose, indicating a more prolonged effect of the 3X tamoxifen dose (Figure 2f).

The comparison of PDGFR $\beta^+$  cell ablation in the cortex between the acute and chronic phases revealed a partial recovery in both pericyte coverage and numbers during the chronic phase. This recovery was most notable in the 2X dose group, where pericyte numbers increased from 42% to 69% of the control group and pericyte coverage improved from 17% to 33% (Figure 2g,h). The 3X group also showed some recovery, with coverage increasing from 19% in the acute phase to 29% in the chronic phase (Figure 2g). However, pericyte numbers remained stable in the 3X dose group, suggesting a diminished capacity for replenishment as the tamoxifen dose increases (Figure 2h). These findings suggest that CNS pericytes have the ability to partially regenerate over time following acute ablation.

Analysis of pericytes in the spinal cord confirmed the effectiveness of our PDGFR $\beta^+$  cell ablation model in this CNS region as well (Figure 3a,b). In the acute phase, pericyte coverage in the gray matter was reduced to 47%, 64%, and 30% of control levels following 2X, 3X, and 5X tamoxifen doses, respectively (Figure 3c). Similarly, in the white matter, pericyte coverage decreased to 36%, 62%, and 17% of control levels for the 2X, 3X, and 5X doses, respectively (Figure 3d). In all, 60 days after tamoxifen administration, pericyte coverage remained reduced in both the gray and white matters of the 2X group and in the white matter of the 3X group compared to controls (Figure 3c,d).

Pericyte numbers were also decreased in the spinal cord after tamoxifen administration (Figure 3e,f). On Day 15, this

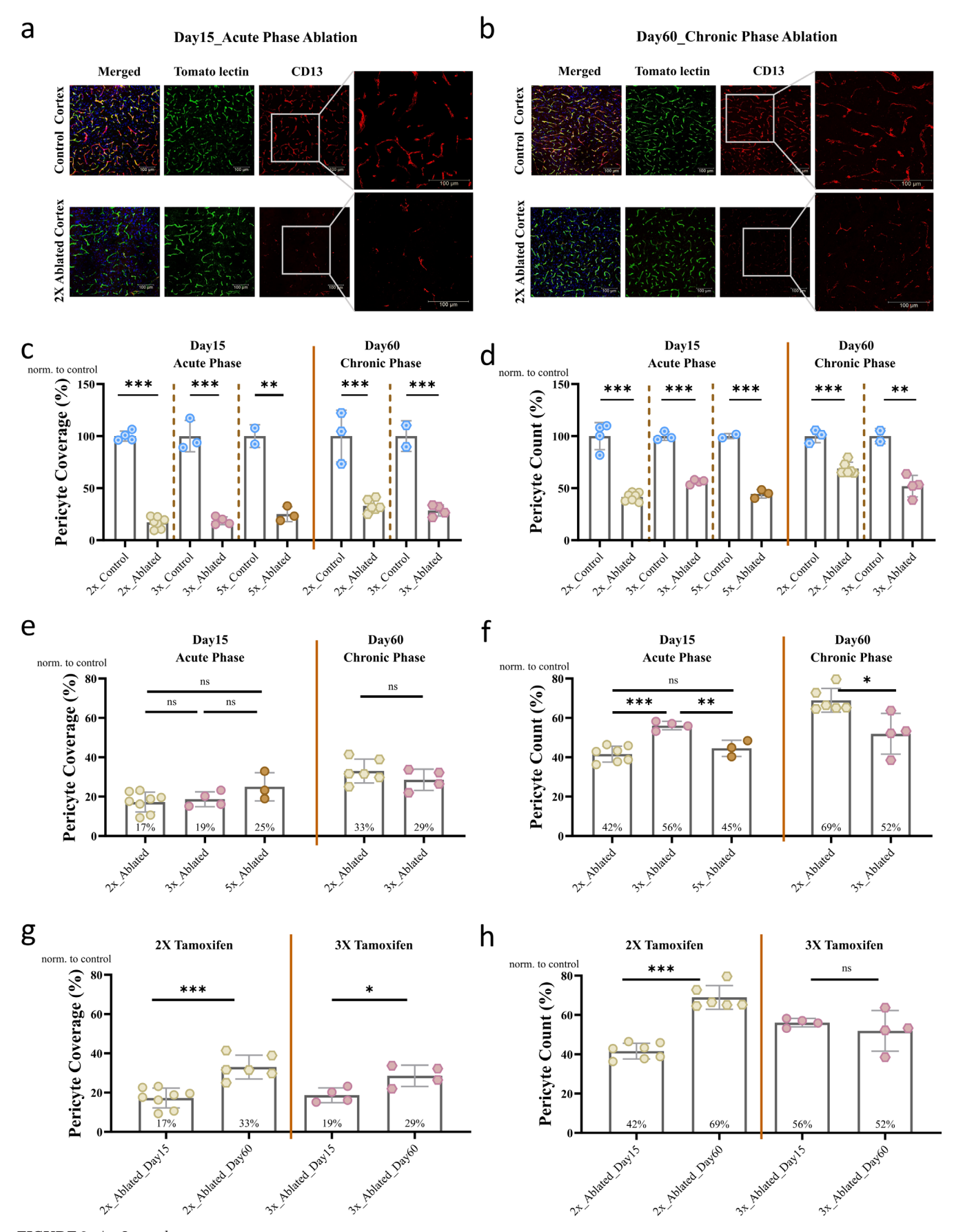
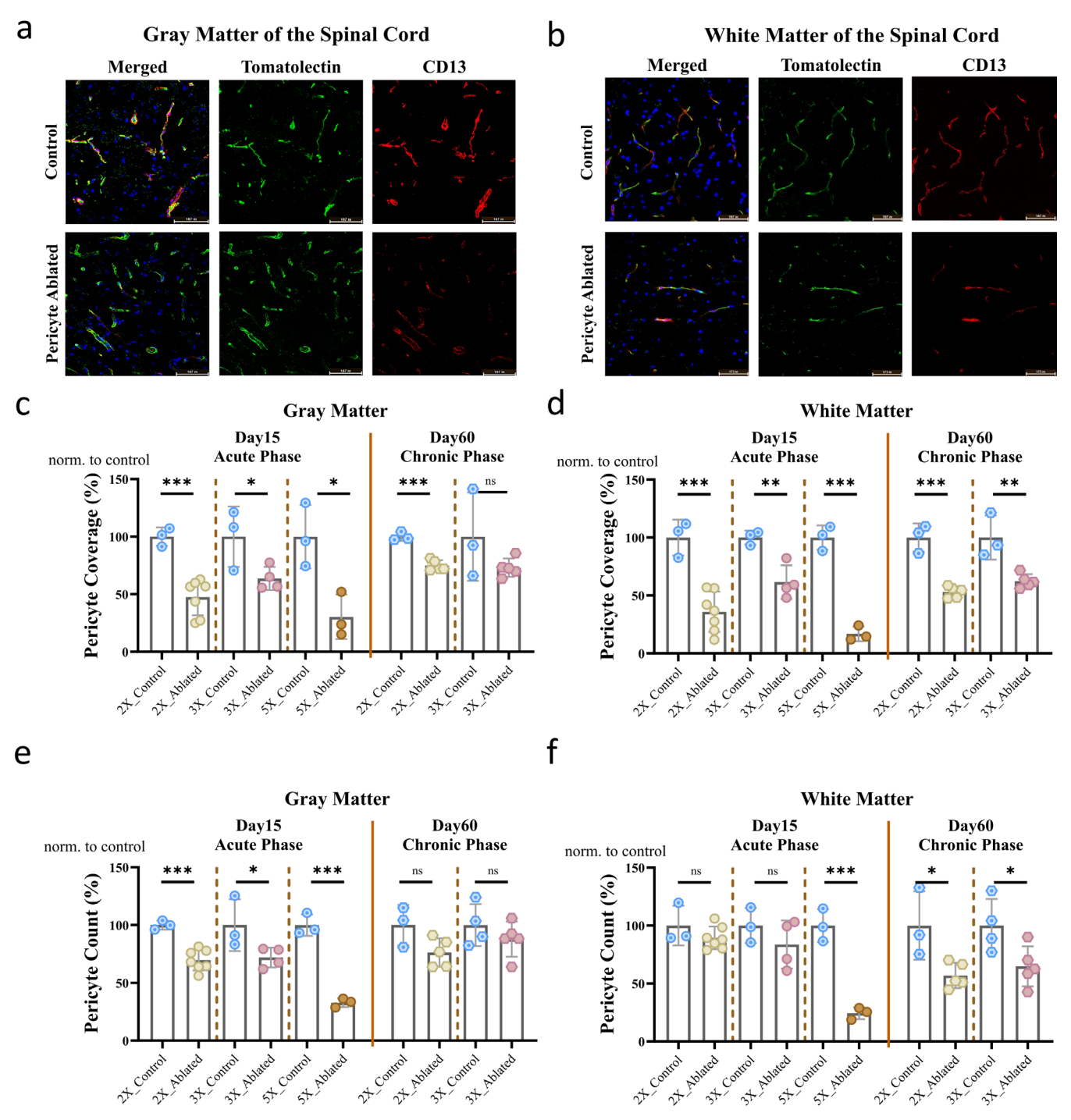


FIGURE 2 | Legend on next page.

FIGURE 2 | Immunofluorescent characterization of PDGFRβ<sup>+</sup> cell ablation in murine cortex. (a, b) Immunofluorescence images showcasing pericytes (CD13, red), blood vessels (tomato lectin, green), and nuclei (Hoechst, blue) within the cortex at acute (Day 15) and chronic (Day 60) phases post-tamoxifen induction, evidencing a significant pericyte loss. (c–h) Quantitative analysis of pericyte coverage (e, g) and count (f, h), demonstrating dose-dependent (e, f) and time-course effects (g, h) of tamoxifen-induced ablation. Statistical significance determined by the Student's *t*-test, with *p*-value annotations: ns (0.1234), \* (0.0332), \*\* (0.0021), and \*\*\* (0.0002). Statistical details are given in Table S4. Data points reflect averages of six to eight cortical images per animal. X = repetitive doses of tamoxifen injection.



**FIGURE 3** | Region-specific effects of PDGFRβ<sup>+</sup> cell ablation in the spinal cord compared to controls. (a, b) Immunofluorescent staining of spinal cord sections (gray matter and white matter, respectively) post-2X tamoxifen induction, revealing stark pericyte coverage reduction. (c-f) Histograms quantifying pericyte coverage and count in gray and white matter, after acute and chronic phases of PDGFRβ<sup>+</sup> cell ablation. Statistical analysis via the Student's *t*-test; *p* values classified as ns (0.1234), \*(0.0332), \*\*(0.0021), and \*\*\*(0.0002). Statistical details are given in Table S5. Data points represent the averages based on 8–10 images from various spinal cord segments per animal. X = repetitive doses of tamoxifen injection.

decrease was evident only in the gray matter but not in white matter of the 2X and 3X tamoxifen groups, whereas the pericyte count was lower in both the gray and white matters of the 5X tamoxifen group compared to controls (Figure 3e,f). On Day 60, similar amounts of pericyte numbers compared to the acute phase were observed in the gray matter of the 2X and 3X tamoxifen groups, and the difference lost its significance compared to their controls (Figure 3e), whereas in the white matter, both the 2X and 3X tamoxifen groups had significantly lower pericyte counts in the chronic phase compared to both controls and the numbers in the acute phase (Figure 3f). These findings suggest that the dynamics of pericyte loss differ between these regions.

When we compared the effect of different doses, the 5X dose resulted in a greater reduction in pericyte coverage and numbers compared to the 2X and 3X doses in the spinal cord gray matter (Figure 4a,c). In the white matter, the 2X and 5X dosages induced a significantly greater reduction in pericyte coverage compared to the 3X tamoxifen dose (Figure 4b), and the 5X dose resulted in a greater reduction in pericyte numbers compared to the 2X and 3X doses (Figure 4d).

Next, we evaluated the capacity for pericyte coverage and number to recover in the spinal cord following acute ablation. In all, 60 days after tamoxifen induction, we observed an increase in pericyte coverage in the gray matter, with a similar upward trend in the white matter in the 2X tamoxifen group compared to Day 15 (Figure 4e,f). Interestingly, this increase in pericyte coverage occurred without a corresponding rise in pericyte counts. These data suggest that changes in pericyte distribution or morphology, such as extended processes or altered cell shapes, may contribute to the increased coverage without altering the overall cell number (Berthiaume et al. 2018). In contrast, pericyte coverage in the 3X tamoxifen group remained unchanged in both the gray and white matters when compared to Day 15. For pericyte counts, no change was detected in the gray matter, while a decrease was noted in the white matter of the 2X tamoxifen group during the chronic phase compared to the acute phase (Figure 4g,h). No statistically significant changes in pericyte counts were observed in the 3X group during the chronic phase.

These analysis also indicated that the extent of pericyte loss is greater in the cortex than in the spinal cord (Figure S5), with more prolonged pericyte deficiency observed in the white matter of the spinal cord compared to the gray matter. Additionally, cortical pericytes exhibit a higher amount of partial recovery rate than those in the spinal cord.

# 3.3 | Vascular Parameters Are Not Changed After Acute PDGFRβ<sup>+</sup> Cell Ablation

Vessel percentage area (VPA), junction density (JD), and average vessel length (AVL) were assessed in the cortex and spinal cord in the acute and chronic phases following 2X tamoxifen administration. There was no statistically significant change in VPA, JD, and AVL in the cortex (Figure 5a–c) and the spinal cord (Figure 5d–i), indicating that inducible PDGFR $\beta$ + cell ablation does not significantly alter vascular morphology up to 60 days in the CNS.

# 3.4 | PDGFRβ<sup>+</sup> Cell Ablation in Adult Mice Does Not Impair Spatial Memory or Muscle Strength

Motor function was evaluated using Kondziela's inverted screen test, and spatial memory was assessed through the Y-maze spontaneous alternation task. These specific tests were selected due to the recognized role of PDGFR $\beta^+$  pericytes in proper neurovascular unit functioning, which has been shown to be fundamentally linked to spatial memory and motor performance (Montagne et al. 2015; Winkler et al. 2014; Sengillo et al. 2013).

Specifically, Kondziela's inverted screen test was selected for motor function assessment based on the connection between pericyte deficiency and motor neuron health seen in amyotrophic lateral sclerosis (ALS) models (Sweeney et al. 2016; Winkler, Sengillo, Sullivan, et al. 2012; Sasaki 2015). In the Kondziela's inverted screen test, the fall time for mice was comparable to controls across all groups, both in acute and chronic phases (Figure 6a), with no significant differences noted across varying tamoxifen doses or time points (Figure 2c,e).

Similarly, in the Y-maze, the spontaneous alternation task specifically evaluates spatial memory, which relies on the hippocampus and its associated neural circuits (Wirt and Hyman 2017). Research with the constitutional models has shown that disruptions in these circuits due to pericyte dysfunction correlate with poorer performance in spatial memory tasks (Kisler et al. 2017; Uemura et al. 2020). In our acute model, however, PDGFR $\beta^+$  cell ablation did not significantly affect spatial memory performance in any group during either phase (Figure 6b), and comparisons across different doses and time points also revealed no significant differences (Figure 6d,f).

# 4 | Discussion

In this study, we present a novel tamoxifen-inducible acute PDGFRβ+ cell ablation model based on the induction of an attenuated diphtheria toxin variant (DTA176) production in Pdgfrβ-expressing cells. Using this model, we have demonstrated that substantial PDGFRβ+ cell depletion within the CNS can be achieved without adversely affecting animal health by precise tamoxifen dosage adjustment (Figure 1). This model enables highly specific and efficient ablation of PDGFR $\beta$ <sup>+</sup> cells, including pericytes, while avoiding nonspecific effects associated with DT injection used in other models. Additionally, we observed that PDGFR $\beta^+$  cells regenerate in vivo, and pericyte coverage is restored in the subsequent weeks following extensive pericyte loss, reinforcing the concept of pericyte plasticity (Figures 2 and 3). Moreover, our findings indicate that the extent of PDGFR $\beta^+$  cell ablation differs between the brain and spinal cord, suggesting regional heterogeneity in pericyte density and dynamics across the CNS.

The model proposed here is based on two transgenic strains:  $PDGFR\beta$ -P2A- $CreER^{T2}$  and Rosa26-DTA176. The  $PDGFR\beta$ -P2A- $CreER^{T2}$  strain, developed by Cuervo et al. (2017), has been previously utilized to study pericytes in the retina, brain, and

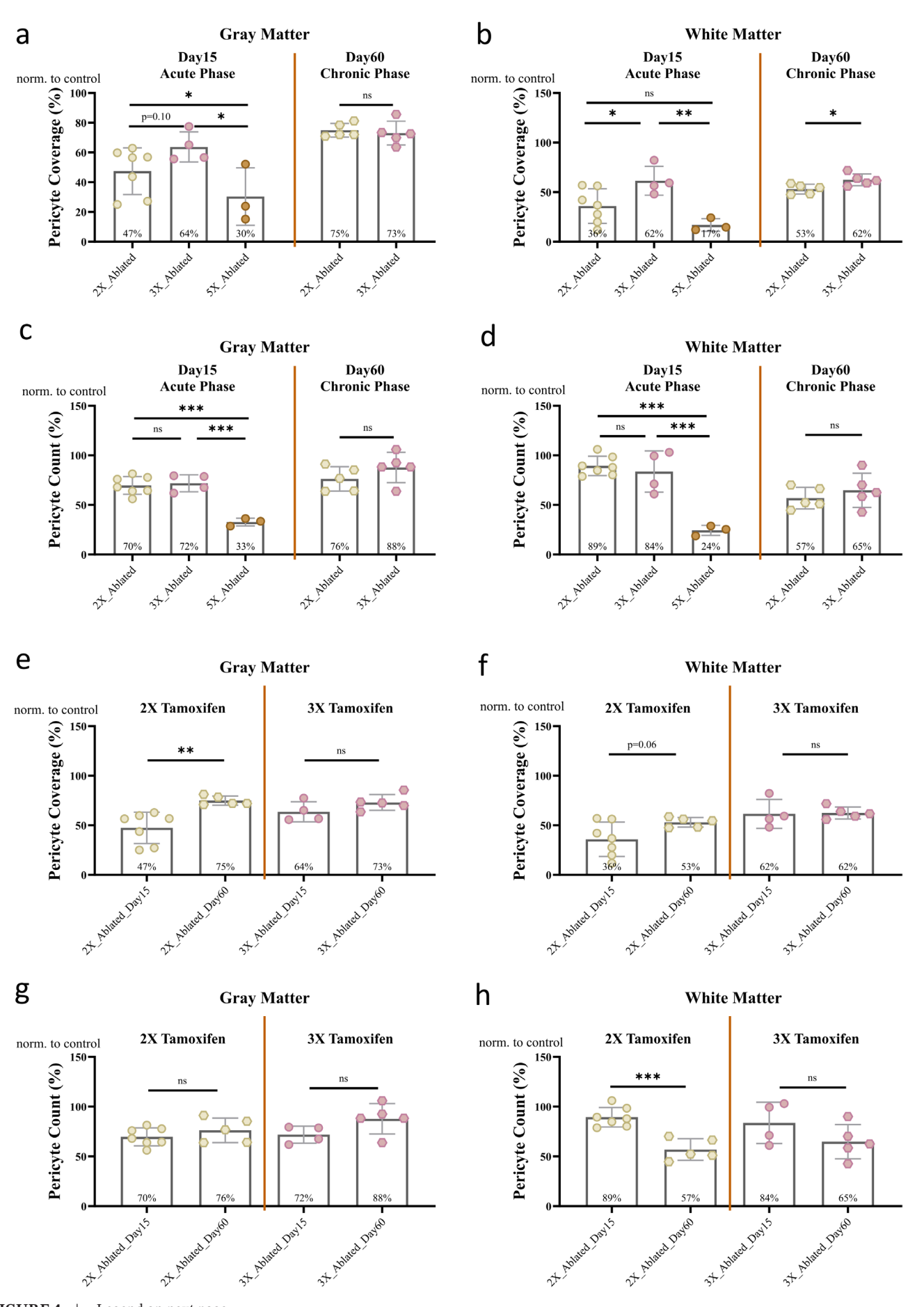


FIGURE 4 | Legend on next page.

**FIGURE 4** Pericyte analysis in the spinal cord across tamoxifen doses. (a–d) Comparison of pericyte coverage (a, b) and pericyte numbers (c, d) in gray matter (a, c) and white matter (b, d) at acute (Day 15) and chronic (Day 60) phases post-tamoxifen across all tamoxifen doses. (e–h) Comparisons of pericyte coverage (e, f) and pericyte number (g, h) in acute and chronic phases for 2X and 3X tamoxifen doses in gray matter (e, g) and white matter (f, h). Statistical significance was assessed via the Student's *t*-test as ns (0.1234), \* (0.0332), \*\* (0.0021), and \*\*\* (0.0002). Statistical details are given in Table S6. Data are taken from multiple spinal cord sections per animal. X = repetitive tamoxifen doses. Data points represent the averages based on 8–10 images from various spinal cord segments per animal. X = repetitive doses of tamoxifen injection.

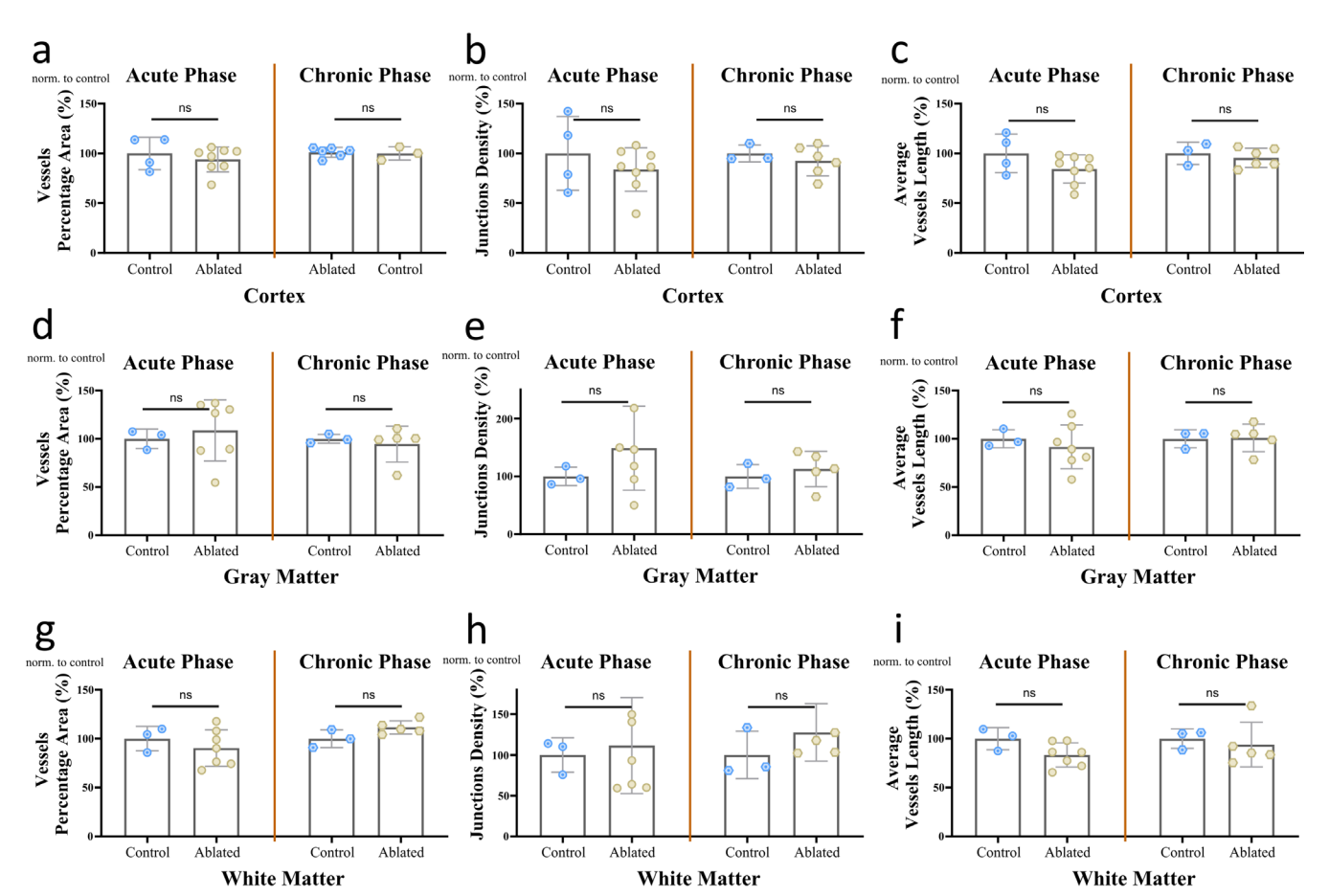


FIGURE 5 | Vascular parameter quantification post-PDGFRβ<sup>+</sup> cell ablation in cortex and spinal cord. A comprehensive evaluation of vascular parameters (vessel percentage area [VPA], junction density [JD], and average vessel length [AVL]) in the cortex and spinal cord during acute and chronic phases postablation with two repetitive doses of tamoxifen induction. Statistical analysis was performed using the Student's *t*-test; significance is denoted as ns (not significant, p=0.1234), \* (p=0.0332), \*\* (p=0.0021), and \*\*\* (p=0.0002). Statistical details are given in Table S7. Data aggregated from 6–8 (cortex) and 10–12 (spinal cord) randomized images per animal.

lung (Ivanova et al. 2021; Teske et al. 2023; Del Narvaez Pilar et al. 2022). By crossing with *Rosa-tdTomato* mice, Cuervo et al. demonstrated tdTomato reporter expression in 84% of NG2-expressing pericytes within the retinal vasculature. In our study, we observed a 75%–83% reduction in cortical pericytes (Figure 2c,d), indicating that DTA176 induction occurred in approximately 80% of pericytes, consistent with Cuervo et al.'s findings.

Previously, Eilken et al. (2017) developed the  $Pdgfr\beta$ - $CreER^{T2}$  mice, which they crossed with ROSA-DTA mice (Voehringer et al. 2008) to create a tamoxifen-inducible acute pericyte ablation model ( $DTA^{\rm IPC}$ ). This model resulted in severe weight loss postnatally, with animals failing to survive beyond 1 week. To mitigate this, Buch et al. utilized the Rosa26-iDTR (Buch et al. 2005), which expresses the DT receptor post-tamoxifen

administration and requires subsequent DT injection for pericyte ablation ( $DTR^{\mathrm{iPC}}$ ). While effective, this system is associated with significant systemic inflammation due to the need for exogenous toxin injections, as reported previously (Bruttger et al. 2015). Our model eliminates this complication by using the intrinsic production of an attenuated DTA176 toxin. Therefore, it could be a safer alternative with a reduced likelihood of systemic inflammatory effects. The lack of exogenous toxin injections makes our model more applicable to studies of neurovascular and inflammatory processes.

In our model, we observed weight loss with 3X and 5X tamoxifen doses but not with the 2X dose. Furthermore, we noted reduced survival rates for 2weeks post-5X tamoxifen administration, an effect absent with lower doses (Figure 1). These observations suggest that acute ablation of PDGFR $\beta^+$  cells systemically

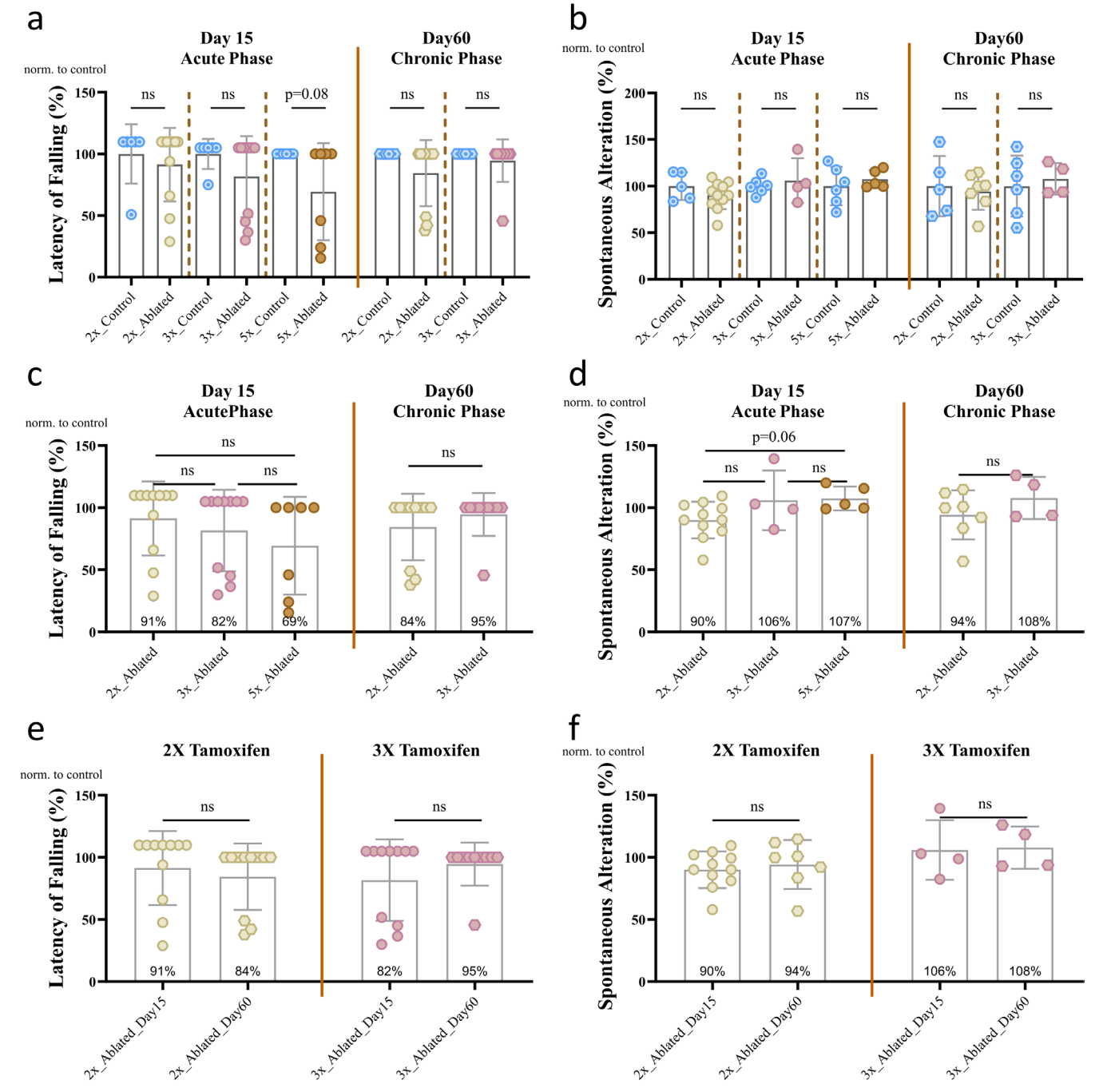


**FIGURE 6** | Motor and cognitive functional assessments following PDGFR $\beta^+$  cell ablation. (a, b) Motor coordination and cognitive function were assessed using the inverted screen test and Y maze spontaneous alternation task, respectively, in mice following tamoxifen-induced PDGFR $\beta^+$  cell ablation. Results across acute and chronic phases are compared for control versus PDGFR $\beta^+$  cell-ablated groups at tamoxifen dosages of 2X, 3X, and 5X. (c, d) Analysis in the chronic phase, incorporating both motor coordination and cognitive assessments, further evaluates the effects of varying tamoxifen doses, highlighting dose-dependent impacts on function. (e, f) Longitudinal comparison of motor and cognitive performance, specifically contrasting the effects of two and three tamoxifen doses across acute and chronic phase. Statistical relevance assessed via the Student's *t*-test, categorizing significance as not significant (ns, p=0.1234), \* (p=0.0332), \*\* (p=0.0021), and \*\*\* (p=0.0002), with data presented as mean ± SEM. Statistical details are given in Table S8.

may precipitate severe systemic effects, necessitating stringent control of tamoxifen dosage to avoid off-target effects on other PDGFR $\beta^+$  cells. To address this limitation, future studies could explore alternative tamoxifen administration routes, such as intraventricular or intrameningeal injections, to improve CNS specificity and minimize systemic exposure. In our study, as the 2X tamoxifen dose did not induce weight loss and the animals

exhibited no complications or behavioral changes for at least 2 months, this regimen can be ideal for future pericyte ablation studies using systemic tamoxifen administration.

Cornuault et al. (2023) recently employed *DTA*<sup>iPC</sup> mice to investigate pericyte ablation effects on cardiac function in 8-week-old mice. Tamoxifen was administered (50 mg/kg/day)

for 5 consecutive days, and the dose was repeated biweekly to sustain stable pericyte ablation (60% capillary pericyte depletion after two injection series), indicating robust renewal potential of cardiac pericytes. In our study, pericyte renewal was also observed after the lowest tamoxifen dose (100 mg/kg/day for 2 days) within the brain (increasing from 42% to 69% of controls in the cortex), highlighting the renewal potential of CNS pericytes. Similar to Eilken et al. Cornuault et al. reported significant weight loss in pericyte-ablated mice, and their systemic analysis revealed near-total depletion of pericytes in the aorta media, intestinal lacteals, and skeletal muscles, with a significant inverse correlation between the degree of cardiac pericyte depletion and weight loss. Consistently, we also observed significant weight loss, severe intestinal pathology, and decreased survival with the 5X tamoxifen dosage. These results demonstrate that the tamoxifen dose must be carefully adjusted and lower doses should be administered to avoid serious systemic effects in  $Pdgfr\beta$ -dependent acute pericyte ablation models.

To circumvent both the developmental problems of the constitutional pericyte deficiency models and to generate a more specific model for brain pericytes, Nikolakopoulou et al. developed a double-promoter approach with Pdgfrβ and Cspg4 (Nikolakopoulou et al. 2019). In this model, pericyte-specific Pdgfrβ-Flp, Cspg4-FSF-CreER mice were crossed with iDTR mice (Buch et al. 2005), and pericyte ablation was induced by 7 days of tamoxifen administration (40 mg/kg/day) followed by 10 days of DT administration (0.1 µg/day) commencing 2 weeks post-tamoxifen. This model achieved 60% pericyte ablation in the cortex 15 days after the final injection. However, this model's limitations include the requirement for repeated DT injections that can be related to potential off-target effects and the limited commercial availability of double-promoter mice. In contrast, our model offers a toxin-free alternative with equivalent ablation efficiency while also being simpler to implement and more accessible for studying pericyte dynamics in adult CNS tissue.

Another tamoxifen-inducible pericyte ablation strategy, as employed by Vazquez-Liebanas et al. (2022) involves the conditional knockout of Pdgfb from Cdh5-expressing endothelial cells. In this model, Pdgfb deletion in 2-month-old mice induces gradual pericyte loss, resulting in a 50% reduction in pericytes by 12–18 months of age. Unlike  $Pdgfr\beta$ - or double-promoter-based models, pericyte loss in this model is not immidiate and exhibits less controllability. In comparison, our model facilitates rapid and robust pericyte ablation, making it particularly suited for investigating acute PDGFR $\beta$ + cell dynamics and their immediate consequences.

We observed a lower reduction in pericyte numbers and coverage following tamoxifen administration in the spinal cord gray and white matter compared to the cortex (Figure S5). Pericyte coverage and number in the spinal cord were previously quantified by Winkler, Sengillo, Bell, et al. (2012). The authors reported that PDGFR $\beta^+$  pericyte coverage was approximately 80%, and pericyte density was around 2000/mm² in the cortex. In the spinal cord anterior horn, both pericyte coverage (~55%) and density (~1100/mm²) were lower compared to the brain, and in the spinal cord white matter (~70% and ~1800/mm², respectively). In the same study,  $Pdgfr\beta^{F7/F7}$  mice (Tallquist et al. 2003) were used to assess the extent of spinal cord PDGFR $\beta^+$  cell

ablation, revealing a ~40% reduction in the anterior horn, which was less pronounced compared to the 60% loss observed in the cortex (Bell et al. 2010). This suggests that the reduced degree of PDGFR $\beta^+$  cell ablation observed in our study for the spinal cord may be attributed to the lower baseline presence of pericytes in this region. On the other hand, Goritz et al. (2011) identified two types of pericytes in the spinal cord and brain, one of which contributes to fibrosis post-injury (Holl et al. 2024). Similarly, Birbrair et al. (2014) identified two types of pericytes (Nestin-negative and -positive) across various organs, including the brain and spinal cord. These studies indicate molecular heterogeneity among pericytes in different CNS regions; therefore, it is possible that  $Pdgfr\beta$  expression may be lower in spinal cord pericytes. Future studies are required for a more precise explanation of this aspect.

The temporal characteristics of pericyte coverage and count following acute, inducible PDGFR $\beta$ <sup>+</sup> cell ablation in adult mice have not been investigated before. In our study, we observed that a lower tamoxifen dosage (2X) facilitated partial recovery of both pericyte count and coverage in the cortex during the chronic phase (Figure 2). Conversely, in mice administered a 3X tamoxifen dose, an increase in pericyte coverage, but not pericyte count of cortex, was noted. In the spinal cord gray matter, an increase in pericyte coverage, but not number, was observed after the 2X dose (Figure 4). Previously, utilizing PDGFRβ-Cre/ YFP mice and chronic cranial window imaging, Berthiaume et al. (2018) demonstrated that pericyte processes are dynamic under basal conditions and can extend to contact uncovered endothelial regions following the selective ablation of adjacent pericytes. In a subsequent study, the same group reported that pericyte plasticity is compromised in aged mice (Berthiaume et al. 2022). Our findings indicate that CNS pericytes respond to ablation not only by extending processes to cover endothelial gaps but also by replenishing pericytes following more extensive ablation in vivo in adult mice, developing the concept of plasticity of CNS pericytes further. The source of these replenishing cells remains unclear but could involve the proliferation of residual pericytes or the recruitment of progenitor cells. Further studies using lineage-tracing approaches are needed to identify the cellular origins of regenerated pericytes.

Previously, using the double-promoter mice, Kisler et al. (2020) demonstrated that cortical vascular density remains unchanged 3 days following pericyte ablation in adult mice. Consistent with this finding, we found no significant alterations in VPA, AVL, or JD in the cortex and spinal cord 15 days post-pericyte ablation. Furthermore, we observed that brain vascular morphology is preserved up to 60 days post-induction despite sustained pericyte loss. Similarly, using the inducible Pdgfb knockout model, Vazquez-Liebanas et al. (2022) found that adult-induced pericyte loss does not result in vessel dilation, impaired arteriovenous zonation, or microvascular calcifications, contrary to the effects seen with constitutive Pdgfb loss (Lindahl et al. 1997). Collectively, these findings suggest that while pericytes are essential for prenatal vascular development, they are not critical for the maintenance of the mature vascular network in the nervous system during adulthood. However, it is possible that subtle changes in capillary flow dynamics or BBB permeability, which were not assessed in this study, may occur in the absence of pericytes. Future

investigations should incorporate functional assays, such as in vivo imaging of blood flow or tracer studies, to evaluate BBB integrity to address these questions.

Behavioral analysis in our model revealed no significant deficits in spatial memory or motor function (Figure 6), which contrasts with findings from chronic pericyte depletion models (Montagne et al. 2015; Winkler et al. 2014; Sengillo et al. 2013). These findings suggest that, under acute conditions, PDGFR $\beta^+$  cell ablation does not produce the spatial memory or motor deficits typically associated with chronic pericyte deficiency, highlighting the significance of the timing and duration of pericyte loss in influencing functional outcomes in cognitive and motor domains. Our findings provide a valuable baseline for future studies exploring the long-term effects of pericyte ablation on behavior.

There are some limitations to consider. One of the limitations of our model is the inclusion of vSMCs and fibroblasts in the population of PDGFR $\beta$ <sup>+</sup> cells targeted for ablation. Although this overlap is a common feature of all widely used PDGFRβ-based models (Winkler, Sengillo, Bell, et al. 2012; Bell et al. 2010; Watson et al. 2020; Nikolakopoulou et al. 2019, 2017), distinguishing the specific contributions of pericytes versus vSMCs to observed phenotypes remains a challenge for our study. To address this, we utilized CD13 as an alternative marker in our immunohistochemical analysis, which provided additional specificity and reduced potential confounding effects caused by overlapping molecular markers. Additionally, PDGFRβ<sup>+</sup> cell ablation is not limited to the CNS, and the degree of PDGFR $\beta$ <sup>+</sup> cell ablation can be different in other organs, which should be studied in future studies. As another limitation, while previous research has demonstrated BBB leakage, changes in glial reactivity, and inflammatory responses following induced PDGFRβ+ cell ablation in adult mice, we did not investigate these mechanisms in this study (Nikolakopoulou et al. 2019; Vazquez-Liebanas et al. 2022).

Despite these limitations, our findings significantly advance the understanding of pericyte plasticity and regeneration. Notably, the partial recovery of pericyte coverage and numbers in both the cortex and spinal cord following low-dose tamoxifen administration demonstrates a previously underappreciated regenerative capacity of pericytes in the adult CNS. The timeline of pericyte depletion and partial recovery provides critical insights into the broader implications and utility of this model for studying neurovascular and inflammatory processes in neurological diseases.

In conclusion, our tamoxifen-inducible,  $Pdgfr\beta$  expression–specific pericyte ablation model offers significant improvements in temporal control, specificity and simplicity over existing models. It enables detailed studies of pericyte roles in adult CNS physiology without the developmental confounds of traditional models. This temporal precision also allowed us to perform longitudinal analyses, revealing the regenerative capacity of CNS pericytes and their ability to partially restore coverage and numbers following ablation. Additionally, the tamoxifen-controlled intrinsic DT expression strategy of our model makes it systemically safer compared to other inducible models requiring the exogenous injection of the toxin. Our model's adaptability was

demonstrated by examining regional differences in pericyte dynamics across the cortex, spinal cord gray matter, and white matter, highlighting heterogeneity in pericyte density and ablation efficiency within the CNS. Furthermore, our characterization of three tamoxifen doses identified an optimal 2 consecutive days of injection regimen that achieves effective pericyte depletion while avoiding systemic toxicity or behavioral deficits, enhancing the model's practicality. Beyond CNS studies, this model's versatility extends to other organs with Pdgfrβ-positive cells, providing a valuable tool for exploring pericyte contributions to systemic vascular and inflammatory processes. However, dosedependent toxicity and regional variability highlight the need for careful experimental design and interpretation. This model provides a robust platform for advancing our understanding of mural cell-mediated neurovascular regulation and developing targeted therapeutic strategies for neurovascular disorders.

#### **Author Contributions**

Dila Atak: conceptualization, data curation, formal analysis, investigation, methodology, visualization, writing - original draft. Erdost Yıldız: data curation, formal analysis, methodology. Esra Özkan: data curation, formal analysis. Mohammadreza Yousefi: data curation. Ayşe Özkan: data curation, formal analysis. Aysu Bilge Yılmaz: data curation, formal analysis. Ali Burak Kızılırmak: methodology. Iman Asaad Alnajjar: formal analysis. Çiçek Kanar: methodology. Zeynep Lal Caan: methodology. Şakir Ümit Zeybek: methodology. Cem İsmail Kücükali: conceptualization, funding acquisition, project administration, resources. Erdem Tüzün: conceptualization, funding acquisition, project administration, resources, supervision. Yasemin Gürsoy-Özdemir: conceptualization, data curation, funding acquisition, investigation, methodology, project administration, supervision, writing - review and editing. Atay Vural: conceptualization, data curation, funding acquisition, investigation, methodology, project administration, resources, supervision, writing - review and editing.

# Acknowledgments

This study was conducted using the services and infrastructure of Koç University Research Center for Translational Medicine (KUTTAM).

#### **Data Availability Statement**

The datasets generated and analyzed during this study are available from the corresponding author upon reasonable request. A preprint of this article was posted on bioRxiv on September 28, 2024, and can be accessed at <a href="https://www.biorxiv.org/content/10.1101/2024.09.27.6146">https://www.biorxiv.org/content/10.1101/2024.09.27.6146</a> 65v1.

#### **Peer Review**

The peer review history for this article is available at https://www.webof science.com/api/gateway/wos/peer-review/10.1111/jnc.70035.

#### References

Armulik, A., G. Genove, and C. Betsholtz. 2011. "Pericytes: Developmental, Physiological, and Pathological Perspectives, Problems, and Promises." *Developmental Cell* 21: 193–215. https://doi.org/10.1016/j.devcel.2011.07.001.

Armulik, A., G. Genové, M. Mäe, et al. 2010. "Pericytes Regulate the Blood-Brain Barrier." *Nature* 468: 557–561. https://doi.org/10.1038/nature09522.

Bell, R. D., E. A. Winkler, A. P. Sagare, et al. 2010. "Pericytes Control Key Neurovascular Functions and Neuronal Phenotype in the Adult Brain and During Brain Aging." *Neuron* 68, no. 3: 409–427. https://doi.org/10.1016/j.neuron.2010.09.043.

Berthiaume, A.-A., R. I. Grant, K. P. McDowell, et al. 2018. "Dynamic Remodeling of Pericytes in Vivo Maintains Capillary Coverage in the Adult Mouse Brain." *Cell Reports* 22: 8–16. https://doi.org/10.1016/j.cel-rep.2017.12.016.

Berthiaume, A. A., F. Schmid, S. Stamenkovic, et al. 2022. "Pericyte Remodeling Is Deficient in the Aged Brain and Contributes to Impaired Capillary Flow and Structure." *Nature Communications* 13: 5912. https://doi.org/10.1038/s41467-022-33464-w.

Birbrair, A., T. Zhang, D. C. Files, et al. 2014. "Type-1 Pericytes Accumulate After Tissue Injury and Produce Collagen in an Organ-Dependent Manner." *Stem Cell Research & Therapy* 5: 122. https://doi.org/10.1186/scrt512.

Bruttger, J., K. Karram, S. Wörtge, et al. 2015. "Genetic Cell Ablation Reveals Clusters of Local Self-Renewing Microglia in the Mammalian Central Nervous System." *Immunity* 43: 92–106. https://doi.org/10.1016/j.immuni.2015.06.012.

Buch, T., F. L. Heppner, C. Tertilt, et al. 2005. "A Cre-Inducible Diphtheria Toxin Receptor Mediates Cell Lineage Ablation After Toxin Administration." *Nature Methods* 2: 419–426. https://doi.org/10.1038/nmeth762.

Cornuault, L., F. X. Hérion, C. Bourguignon, et al. 2023. "Partial Mural Cell Ablation Disrupts Coronary Vasculature Integrity and Induces Systolic Dysfunction." *Journal of the American Heart Association* 12: e029279. https://doi.org/10.1161/JAHA.122.029279.

Crouch, E. E., C. Liu, V. Silva-Vargas, and F. Doetsch. 2015. "Regional and Stage-Specific Effects of Prospectively Purified Vascular Cells on the Adult V-SVZ Neural Stem Cell Lineage." *Journal of Neuroscience* 35: 4528–4539. https://doi.org/10.1523/jneurosci.1188-14.2015.

Cuervo, H., B. Pereira, T. Nadeem, et al. 2017. "PDGFRβ-P2A-CreERT2 Mice: A Genetic Tool to Target Pericytes in Angiogenesis." *Angiogenesis* 20, no. 4: 655–662. https://doi.org/10.1007/s10456-017-9570-9.

Daneman, R., L. Zhou, A. A. Kebede, and B. A. Barres. 2010. "Pericytes Are Required for Blood-Brain Barrier Integrity During Embryogenesis." *Nature* 468: 562–566. https://doi.org/10.1038/nature09513.

Del Narvaez Pilar, O., M. J. Gacha Garay, and J. Chen. 2022. "Three-Axis Classification of Mouse Lung Mesenchymal Cells Reveals Two Populations of Myofibroblasts." *Development* 149, no. 6: dev200081. https://doi.org/10.1242/dev.200081.

Eilken, H. M., R. Diéguez-Hurtado, I. Schmidt, et al. 2017. "Pericytes Regulate VEGF-Induced Endothelial Sprouting Through VEGFR1." *Nature Communications* 8: 1574. https://doi.org/10.1038/s41467-017-01738-3.

Enge, M., M. Bjarnegård, H. Gerhardt, et al. 2002. "Endothelium-Specific Platelet-Derived Growth Factor-B Ablation Mimics Diabetic Retinopathy." *EMBO Journal* 21: 4307–4316. https://doi.org/10.1093/emboj/cdf418.

Goritz, C., D. O. Dias, N. Tomilin, M. Barbacid, O. Shupliakov, and J. Frisén. 2011. "A Pericyte Origin of Spinal Cord Scar Tissue." *Science* 333: 238–242. https://doi.org/10.1126/science.1203165.

Hall, C. N., C. Reynell, B. Gesslein, et al. 2014. "Capillary Pericytes Regulate Cerebral Blood Flow in Health and Disease." *Nature* 508, no. 7494: 55–60. https://doi.org/10.1038/nature13165.

Hartmann, D. A., A.-A. Berthiaume, R. I. Grant, et al. 2021. "Brain Capillary Pericytes Exert a Substantial but Slow Influence on Blood Flow." *Nature Neuroscience* 24, no. 5: 633–645. https://doi.org/10.1038/s41593-020-00793-2.

Holl, D., W. F. Hau, A. Julien, et al. 2024. "Distinct Origin and Region-Dependent Contribution of Stromal Fibroblasts to Fibrosis Following Traumatic Injury in Mice." *Nature Neuroscience* 27: 1285–1298. https://doi.org/10.1038/s41593-024-01678-4.

Ivanova, E., C. Corona, C. G. Eleftheriou, P. Bianchimano, and B. T. Sagdullaev. 2021. "Retina-Specific Targeting of Pericytes Reveals Structural Diversity and Enables Control of Capillary Blood Flow." *Journal of Comparative Neurology* 529: 1121–1134. https://doi.org/10.1002/cne.25011.

Kaushik, D. K., A. Bhattacharya, B. M. Lozinski, and V. Wee Yong. 2021. "Pericytes as Mediators of Infiltration of Macrophages in Multiple Sclerosis." *Journal of Neuroinflammation* 18: 301. https://doi.org/10.1186/s12974-021-02358-x.

Kisler, K., A. R. Nelson, S. V. Rege, et al. 2017. "Pericyte Degeneration Leads to Neurovascular Uncoupling and Limits Oxygen Supply to Brain." *Nature Neuroscience* 20, no. 3: 406–416. https://doi.org/10.1038/nn.4489.

Kisler, K., A. M. Nikolakopoulou, M. D. Sweeney, D. Lazic, Z. Zhao, and B. V. Zlokovic. 2020. "Acute Ablation of Cortical Pericytes Leads to Rapid Neurovascular Uncoupling." *Frontiers in Cellular Neuroscience* 14: 27. https://doi.org/10.3389/fncel.2020.00027.

Leveen, P., M. Pekny, S. Gebre-Medhin, B. Swolin, E. Larsson, and C. Betsholtz. 1994. "Mice Deficient for PDGF B Show Renal, Cardiovascular, and Hematological Abnormalities." *Genes & Development* 8: 1875–1887. https://doi.org/10.1101/gad.8.16.1875.

Lindahl, P., B. R. Johansson, P. Leveen, and C. Betsholtz. 1997. "Pericyte Loss and Microaneurysm Formation in PDGF-B-Deficient Mice." *Science* 277: 242–245. https://doi.org/10.1126/science.277.5323.242.

Lindblom, P. 2003. "Endothelial PDGF-B Retention Is Required for Proper Investment of Pericytes in the Microvessel Wall." *Genes & Development* 17: 1835–1840. https://doi.org/10.1101/gad.266803.

Montagne, A., S. R. Barnes, M. D. Sweeney, et al. 2015. "Blood-Brain Barrier Breakdown in the Aging Human Hippocampus." *Neuron* 85: 296–302. https://doi.org/10.1016/j.neuron.2014.12.032.

Montagne, A., A. M. Nikolakopoulou, Z. Zhao, et al. 2018. "Pericyte Degeneration Causes White Matter Dysfunction in the Mouse Central Nervous System." *Nature Medicine* 24, no. 3: 326–337. https://doi.org/10.1038/nm.4482.

Nehls, V., K. Denzer, and D. Drenckhahn. 1992. "Pericyte Involvement in Capillary Sprouting During Angiogenesis In Situ." *Cell and Tissue Research* 270: 469–474. https://doi.org/10.1007/BF00645048.

Nikolakopoulou, A. M., A. Montagne, K. Kisler, et al. 2019. "Pericyte Loss Leads to Circulatory Failure and Pleiotrophin Depletion Causing Neuron Loss." *Nature Neuroscience* 22, no. 7: 1089–1098. https://doi.org/10.1038/s41593-019-0434-z.

Nikolakopoulou, A. M., Z. Zhao, A. Montagne, and B. V. Zlokovic. 2017. "Regional Early and Progressive Loss of Brain Pericytes but Not Vascular Smooth Muscle Cells in Adult Mice With Disrupted Platelet-Derived Growth Factor Receptor-Beta Signaling." *PLoS One* 12: e0176225. https://doi.org/10.1371/journal.pone.0176225.

Ozerdem, U., E. Monosov, and W. B. Stallcup. 2002. "NG2 Proteoglycan Expression by Pericytes in Pathological Microvasculature." *Microvascular Research* 63: 129–134. https://doi.org/10.1006/mvre. 2001.2376.

Peppiatt, C. M., C. Howarth, P. Mobbs, and D. Attwell. 2006. "Bidirectional Control of CNS Capillary Diameter by Pericytes." *Nature* 443, no. 7112: 700–704. https://doi.org/10.1038/nature05193.

Rustenhoven, J., D. Jansson, L. C. Smyth, and M. Dragunow. 2017. "Brain Pericytes as Mediators of Neuroinflammation." *Trends in Pharmacological Sciences* 38: 291–304. https://doi.org/10.1016/j.tips. 2016.12.001.

Sagare, A. P., R. D. Bell, Z. Zhao, et al. 2013. "Pericyte Loss Influences Alzheimer-Like Neurodegeneration in Mice." *Nature Communications* 4, no. 1: 2932. https://doi.org/10.1038/ncomms3932.

Sandow, S. L., S. M. Wilson, and M. D. Leo. 2023. "Editorial: The Role of Pericytes in Physiology and Pathophysiology." *Frontiers in Physiology* 14: 1306031. https://doi.org/10.3389/fphys.2023.1306031.

16 of 17

Sasaki, S. 2015. "Alterations of the Blood-Spinal Cord Barrier in Sporadic Amyotrophic Lateral Sclerosis." *Neuropathology* 35: 518–528. https://doi.org/10.1111/neup.12221.

Sekerdag-Kilic, E., C. Ulusoyb, D. Ataka, et al. 2023. "Perivascular PDGFRB+ Cells Accompany Lesion Formation and Clinical Evolution Differentially in Two Different EAE Models." *Multiple Sclerosis and Related Disorders* 69: 104428. https://doi.org/10.1016/j.msard.2022. 104428.

Sengillo, J. D., E. A. Winkler, C. T. Walker, J. S. Sullivan, M. Johnson, and B. V. Zlokovic. 2013. "Deficiency in Mural Vascular Cells Coincides With Blood-Brain Barrier Disruption in Alzheimer's Disease." *Brain Pathology* 23: 303–310. https://doi.org/10.1111/bpa.12004.

Stapor, P. C., R. Sweat, D. Dashti, A. M. Betancourt, and W. L. Murfee. 2014. "Pericyte Dynamics During Angiogenesis: New Insights From New Identities." *Journal of Vascular Research* 51, no. 3: 163–174. https://doi.org/10.1159/000362276.

Sweeney, M. D., S. Ayyadurai, and B. V. Zlokovic. 2016. "Pericytes of the Neurovascular Unit: Key Functions and Signaling Pathways." *Nature Neuroscience* 19: 771–783. https://doi.org/10.1038/nn.4288.

Tallquist, M. D., W. J. French, and P. Soriano. 2003. "Additive Effects of PDGF Receptor Beta Signaling Pathways in Vascular Smooth Muscle Cell Development." *PLoS Biology* 1: E52. https://doi.org/10.1371/journ al.pbio.0000052.

Teske, N. C., S. Dyckhoff-Shen, P. Beckenbauer, et al. 2023. "Pericytes Are Protective in Experimental Pneumococcal Meningitis Through Regulating Leukocyte Infiltration and Blood-Brain Barrier Function." *Journal of Neuroinflammation* 20: 267. https://doi.org/10.1186/s12974-023-02938-z.

Torok, O., B. Schreiner, J. Schaffenrath, et al. 2021. "Pericytes Regulate Vascular Immune Homeostasis in the CNS." *Proceedings of the National Academy of Sciences of the United States of America* 118, no. 10: e2016587118. https://doi.org/10.1073/pnas.2016587118.

Trost, A., S. Lange, F. Schroedl, et al. 2016. "Brain and Retinal Pericytes: Origin, Function and Role." *Frontiers in Cellular Neuroscience* 10: 20. https://doi.org/10.3389/fncel.2016.00020.

Uemura, M., T. Maki, M. Ihara, V. Lee, and T. Jq. 2020. "Brain Microvascular Pericytes in Vascular Cognitive Impairment and Dementia." *Frontiers in Aging Neuroscience* 12: 80. https://doi.org/10.3389/fnagi.2020.00080.

Vanlandewijck, M., M. Vanlandewijck, L. He, et al. 2018. "A Molecular Atlas of Cell Types and Zonation in the Brain Vasculature." *Nature* 554, no. 7693: 475–480. https://doi.org/10.1038/nature25739.

Vazquez-Liebanas, E., K. Nahar, G. Bertuzzi, A. Keller, C. Betsholtz, and M. A. Mäe. 2022. "Adult-Induced Genetic Ablation Distinguishes PDGFB Roles in Blood-Brain Barrier Maintenance and Development." *Journal of Cerebral Blood Flow & Metabolism* 42: 264–279. https://doi.org/10.1177/0271678X211056395.

Voehringer, D., H. E. Liang, and R. M. Locksley. 2008. "Homeostasis and Effector Function of Lymphopenia-Induced 'Memory-Like' T Cells in Constitutively T Cell-Depleted Mice." *Journal of Immunology* 180: 4742–4753. https://doi.org/10.4049/jimmunol.180.7.4742.

Watson, A. N., A.-A. Berthiaume, A. V. Faino, et al. 2020. "Mild Pericyte Deficiency Is Associated With Aberrant Brain Microvascular Flow in Aged PDGFR $\beta$ +/- Mice." *Journal of Cerebral Blood Flow & Metabolism* 40, no. 12: 2387–2400. https://doi.org/10.1177/0271678X19900543.

Winkler, E. A., R. D. Bell, and B. V. Zloković. 2010. "Pericyte-Specific Expression of PDGF Beta Receptor in Mouse Models With Normal and Deficient PDGF Beta Receptor Signaling." *Molecular Neurodegeneration* 5: 32. https://doi.org/10.1186/1750-1326-5-32.

Winkler, E. A., A. P. Sagare, and B. V. Zlokovic. 2014. "The Pericyte: A Forgotten Cell Type With Important Implications for Alzheimer's

Disease?" *Brain Pathology* 24: 371–386. https://doi.org/10.1111/bpa. 12152.

Winkler, E. A., J. D. Sengillo, R. D. Bell, J. Wang, and B. V. Zlokovic. 2012. "Blood-Spinal Cord Barrier Pericyte Reductions Contribute to Increased Capillary Permeability." *Journal of Cerebral Blood Flow and Metabolism* 32: 1841–1852. https://doi.org/10.1038/jcbfm.2012.113.

Winkler, E. A., J. D. Sengillo, J. S. Sullivan, J. S. Henkel, S. H. Appel, and B. V. Zlokovic. 2012. "Blood–Spinal Cord Barrier Breakdown and Pericyte Reductions in Amyotrophic Lateral Sclerosis." *Acta Neuropathologica* 125, no. 1: 111–120. https://doi.org/10.1007/s00401-012-1039-8.

Wirt, R. A., and J. M. Hyman. 2017. "Integrating Spatial Working Memory and Remote Memory: Interactions Between the Medial Prefrontal Cortex and Hippocampus." *Brain Sciences* 7, no. 4: 43. https://doi.org/10.3390/brainsci7040043.

Wu, S., Y. Wu, and M. R. Capecchi. 2006. "Motoneurons and Oligodendrocytes Are Sequentially Generated From Neural Stem Cells but Do Not Appear to Share Common Lineage-Restricted Progenitors In Vivo." *Development* 133: 581–590. https://doi.org/10.1242/dev.02236.

Yemisci, M., Y. Gursoy-Ozdemir, A. Vural, A. Can, K. Topalkara, and T. Dalkara. 2009. "Pericyte Contraction Induced by Oxidative-Nitrative Stress Impairs Capillary Reflow Despite Successful Opening of an Occluded Cerebral Artery." *Nature Medicine* 15, no. 9: 1031–1037. https://doi.org/10.1038/nm.2022.

#### **Supporting Information**

Additional supporting information can be found online in the Supporting Information section.